Loss reduction technique in ferroelectric tunable devices by laser micro-etching. Application to a CPW stub resonator in X-band

Yonathan Corredores, Quentin Simon, Ratiba Benzerga, Xavier Castel, Ronan Sauleau, Arnaud Le Febvrier, Stéphanie Députier, Maryline Guilloux-Viry, Lingyan Zhang, Gérard Tanné

▶ To cite this version:

HAL Id: hal-01069143

https://hal.archives-ouvertes.fr/hal-01069143

Submitted on 5 Jan 2016

Loss Reduction Technique in Ferroelectric Tunable Devices by Laser Microetching. Application to a CPW Stub Resonator in X-Band

Yonathan Corredores, Quentin Simon, Ratiba Benzerga, Xavier Castel, Ronan Sauleau, *Senior Member, IEEE*, Arnaud Le Febvrier, Stéphanie Députier, Maryline Guilloux-Viry, Ling Yan Zhang, and Gérard Tanné

Abstract—**Ferroelectric materials are known to be lossy at microwaves. A local microetching technique based on laser ablation is implemented here to reduce the insertion loss of highly tunable devices fabricated on $KTa_{1-x}Nb_xO_3$ (KTN) ferroelectric thin films. The relevance of this approach is studied in X-band by comparing numerically and experimentally the performance of a frequency-tunable coplanar waveguide stub resonator before and after KTN microetching. The experimental data demonstrate a large loss reduction (by a factor 3.3), while keeping a high-frequency tunability (47%) under a moderate biasing static electric field (80 kV/cm). This approach paves the way for the design of ferroelectric reconfigurable devices with attractive performance in X-band and even beyond.**

Index Terms—**Ferroelectric film, laser etching, tunable resonator.**

I. INTRODUCTION

TUNABLE circuits and antennas are very attractive for future multistandard and multifunction telecommunication systems due to their versatility and miniaturization capabilities [1], [2]. Many devices based on p-i-n [3], [4] or varactor diodes [5], [6] and microelectromechanical system switches [7], [8] have been proposed over the years.

An alternative solution consists in using tunable materials like nematic liquid crystals [9], [10] or ferroelectric materials [1], [11], [12]. As the former may suffer from slow switching time and, sometimes, low tunability at RF and microwaves, we focus our attention on ferroelectric-based solutions. These materials exhibit good power handling

Y. Corredores, Q. Simon, R. Benzerga, X. Castel, and R. Sauleau are with the Institut d'Electronique et de Télécommunications de Rennes, Université de Rennes 1, 35042 Rennes, France (e-mail: xavier.castel@univ-rennes1.fr).

A. Le Febvrier, S. Députier, and M. Guilloux-Viry are with the Institut des Sciences Chimiques de Rennes, Université de Rennes 1, 35042 Rennes, France (e-mail: maryline.guilloux-viry@univ-rennes1.fr).

L. Y. Zhang and G. Tanné are with the Laboratoire des Sciences et Techniques de l'Information, de la Communication et de la Connaissance, Université de Bretagne Occidentale, 29238 Brest, France (e-mail: gerard.tanne@univ-brest.fr).

Color versions of one or more of the figures in this paper are available online at http://ieeexplore.ieee.org.

TABLE I
EXAMPLES OF BST TUNABLE DEVICES

	Center frequency	Tunability (%)	E_{bias} (kV/cm)	Insertion loss (dB)
Filter [16] (based on MIM capacitor)	~400 MHz	9	15	3
CPW stub resonator [17]	~2.5 GHz	12.6	140	5
Filter [18] (based on IDC)	~3 GHz	21	165	3
Slow-wave bandpass filter [19]	~13 GHz	20	100	3
Interdigitated capacitor [21]	~25 GHz	20	60	--

capabilities and large dielectric permittivity, which is desirable for circuit miniaturization. Their permittivity value is controlled by an external static electric field E_{bias}, and thin-film ferroelectric devices can be easily integrated with planar circuits.

The most popular ferroelectric material is the barium strontium titanate family ($Ba_xSr_{1-x}TiO_3$ or BST) [13]. It exhibits attractive characteristics in X-band with dielectric permittivity and loss tangent values typically in the range $\varepsilon_{BST} \approx 500$ and $\tan\delta_{BST} \approx 0.05$, respectively [14], [15]. Many BST reconfigurable devices have been reported so far. Most of them are based on the 60/40 composition ($x = 0.6$), which leads to the paraelectric state of BST at room temperature. Table I provides a set of relevant results in terms of tunability, biasing, and insertion loss, obtained over a wide frequency range. Despite the paraelectric state of the BST, it shows that such devices suffer from significant insertion loss [16]–[19]. Two solutions have been proposed to reduce them: an intrinsic route consists in doping the BST material to decrease its loss tangent ($\tan\delta_{BST}$ varies from 0.013 to 0.007 at 1 MHz after Mg doping [20]), whereas an extrinsic route suggests designing hybrid circuits, for instance by integrating a negative resistance to reduce the device loss by a factor two [21].

In this paper, the attention is focused on an alternative ferroelectric oxide, the potassium tantalate niobate family ($KTa_{1-x}Nb_xO_3$ or KTN). The $KTa_{0.5}Nb_{0.5}O_3$ composition ($x = 0.5$), with a T_C of 97 °C (bulk value) [22], has been specifically selected to reach the highest agility of the dielectric permittivity [23], and therefore, the largest frequency tunability of the device. The choice of this composition also leads to work in the ferroelectric state at room temperature.

Due to irreversibility effects and dynamics of domains that contribute to loss, working in the paraelectric state is often chosen for agile device applications. However, it has been pointed out that at microwaves, it could be of interest to use the ferroelectric material in its ferroelectric state, since at these frequencies the loss due to domain walls dynamics as well as hysteretic properties tends to disappear [24]. The KTN dielectric permittivity in the ferroelectric state is then larger than that of the usually reported BST in X-band ($\varepsilon_{KTN} \approx 700$–$850$ [25], [26]). Therefore, a broader tunability range is expected for KTN-based devices [26], [27] as it has been reported recently for coplanar waveguide (CPW) stub resonator printed on a 600-nm-thick $KTa_{0.5}Nb_{0.5}O_3$ film [25]. Nevertheless, standard KTN-based devices suffer from high-insertion loss due to significant KTN loss tangent at microwaves ($\tan\delta_{KTN} \approx 0.15$–$0.3$ [25], [26]). Two main solutions have been investigated so far to reduce its intrinsic loss: MgO doping [28], and improvement of the KTN crystalline quality through the use of suitable seed layer [29]. However, these two approaches still lead to significant loss ($\tan\delta_{KTN} = 0.079$ [28] and $\tan\delta_{KTN} = 0.042$ [29] measured at 12.5 GHz on $KTa_{0.65}Nb_{0.35}O_3$ thin films).

The solution introduced here to further reduce the insertion loss of the KTN devices studied in [25] aims at confining the ferroelectric KTN material only in efficient regions of the device and to remove it in noncritical areas. An original fabrication process based on laser local microetching of the KTN layer has been developed for this purpose. A simple test device, namely, a CPW stub resonator, has been designed and characterized in X-band to demonstrate the relevance of this approach. Note that the proposed route has been already implemented in [30] with a ring resonator in gold printed on an etched strontium titanate (STO) film, but never on KTN. Unfortunately, the technique used in [30] is not specified by the authors (e.g., dry or wet etching process).

This paper is organized as follows. The impact of KTN confinement upon the performance of the stub resonator (tunability and insertion loss) is studied numerically in Section II. The proposed fabrication process is described in Section III, and experimental results obtained before and after KTN etching are discussed in Section IV. Finally, the conclusion is drawn in Section V.

II. NUMERICAL RESULTS

The geometry of the coplanar quarter-wavelength open-ended stub resonator is shown in Fig. 1. This band-rejection filter configuration has been selected for its simple biasing scheme and easiness to quantify the agility induced by the ferroelectric film (change of the resonance frequency). The length of both 50-Ω transmission lines on each side of the stub equals 4 mm. The resonator is fabricated on R-plane sapphire substrate ($\varepsilon_s = 10$; $\tan\delta_s = 10^{-4}$; and thickness $t_s = 0.5$ mm) coated with a KTN underlayer ($t_{KTN} = 1.1$ μm) and a silver metallic overlayer ($t_{Ag} = 2$ μm; conductivity $\sigma_{Ag} = 6.1 \times 10^7$ S/m). The scattering parameters of this resonator are computed with Ansoft high frequency structure simulator (HFSS). In all of the simulations, the dielectric
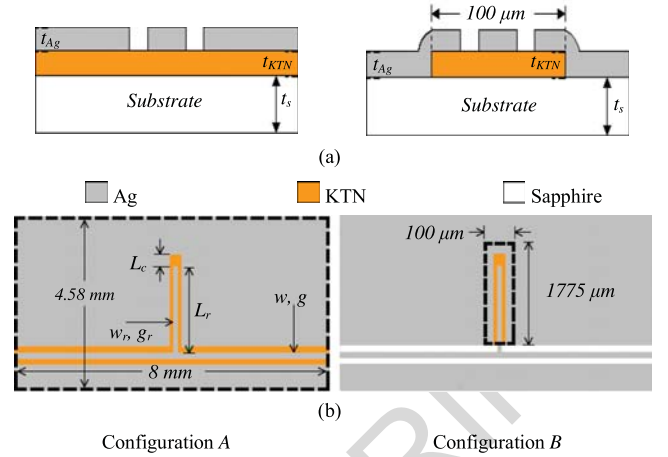

Fig. 1. Geometry and dimensions of the CPW stub resonator. Two configurations are compared here: the dashed lines define the area where KTN is located. $(w, g) = (40, 50)$ μm; $(w_r, g_r) = (14, 14)$ μm; $L_r = 1.52$ mm; and $L_c = 0.1$ mm. (a) Cross-sectional view for the stub. (b) Top view.

permittivity of KTN ε_{KTN} varies from 700 ($E_{bias} = 0$) to 200 (when E_{bias} is applied) [26]; its loss tangent $\tan\delta_{KTN}$ is set to 0.25 [25].

Two configurations are considered and compared in order to highlight the impact of KTN confinement [Fig. 1(a) and (b)]. In these figures, the area where KTN is located is bounded by the dashed-line contours. In both cases, the stub dimensions are the same ($w_r = g_r = 14$ μm; $L_r = 1.52$ mm). Configuration A is the reference one: in this case, the whole sapphire substrate is covered by the KTN layer. In configuration B, the KTN film is localized over a limited area (100 μm $\times$ 1775 μm), only underneath the resonant stub. Simulations have shown that enlarging slightly this area does not impact the results. Indeed most of the field lines are confined close to the stub region.

The metrics used to compare these configurations are the following: the reflection and transmission coefficients S_{11} and S_{21}, the frequency tunability T, and the global loss GL at resonance. T and GL are defined as follows [31]:

$$T(\%) = \left| \frac{F_r(0 \text{ kV/cm}) - F_r(E_{bias})}{F_r(0 \text{ kV/cm})} \right| \times 100 \qquad (1)$$

$$GL = 1 - |S_{11}|^2 - |S_{21}|^2 \qquad (2)$$

where F_r (E_{bias}) is the resonance frequency under external applied dc bias field E_{bias}.

The results computed at resonance for $\varepsilon_{KTN} = 700$ and 200 are shown in Table II. The reflection and transmission coefficients are compared in Fig. 2 for the two configurations. In both cases, the resonance frequency is shifted from $\sim$7.5 GHz for $\varepsilon_{KTN} = 700$ to $\sim$12 GHz for $\varepsilon_{KTN} = 200$. The slight shift in resonance observed under biasing in Fig. 2(b) between configurations A and B comes from the different effective permittivity values of the main transmission line, with and without KTN underlayer. It is worthwhile to note that the insertion loss decreases drastically when KTN is confined under the stub resonator (configuration B). Finally, the increase of loss observed beyond 15 GHz

TABLE II
RESONANCE FREQUENCY F_r, REFLECTION COEFFICIENT
S_{11}, GL, AND TUNABILITY T FOR CONFIGURATIONS
A AND B (NUMERICAL RESULTS)

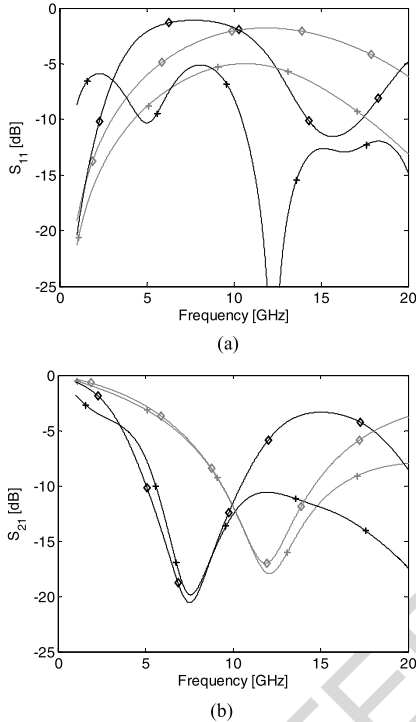| Config.	$\varepsilon_{KTN} = 700$			$\varepsilon_{KTN} = 200$			T (%)
	F_r(GHz)	S_{11} @ F_r (dB)	GL @ F_r	F_r(GHz)	S_{11} @ F_r (dB)	GL @ F_r	
A (ref.)	7.6	-5.5	0.7	12.0	-6.0	0.7	58
B	7.4	-1.0	0.2	11.5	-1.5	0.3	55

Fig. 2. (a) Reflection S_{11} and (b) transmission S_{21} coefficients computed with HFSS for configurations A (+) and B (◊). Black lines: $\varepsilon_{KTN} = 700$. Grey lines: $\varepsilon_{KTN} = 200$. In both cases: $\tan\delta_{KTN} = 0.25$.

is due to the dielectric loss of the ferroelectric material itself [25].

III. FABRICATION PROCESS

A. Deposition of the Ferroelectric Layer

A 1100-nm thick $KTa_{0.5}Nb_{0.5}O_3$ film has been deposited at 700 °C by pulsed laser deposition (PLD) on R-plane sapphire substrate (10 mm × 10 mm × 0.5 mm) using a KrF excimer laser ($\lambda = 248$ nm, 2 Hz) with a laser fluence of 2 J/cm². According to X-ray diffraction analysis, the KTN film is textured and mainly (100) oriented. Using a thick layer (1100 nm) provides a large frequency tunability, but also leads to strong loss. That is, why this sample has been specifically selected: it emphasizes the impact of localizing KTN only in critical regions of the device under test.

B. Fabrication of the CPW Resonator Before Laser Microetching (Configuration A)

A thin titanium film (5-nm-thick) and a 2-μm thick silver overlayer were deposited by RF sputtering at room temperature on the KTN layer. The titanium film ensures a strong adhesion of the silver metallization. The silver thickness is three times larger than the skin depth ($\delta = 0.64$ μm) at 10 GHz. Then standard photolithography and wet-etching processes are implemented to pattern the device. The nominal dimensions of the resonator are provided in Fig. 1. Gold wire bondings are used to enforce the equipotential condition on both CPW grounds and prevent from the excitation of parasitic slotline mode.

C. Fabrication of the CPW Resonator After Laser Microetching (Configuration B)

Once configuration A has been characterized experimentally in reflection and transmission (Section IV), the titanium and silver layers were removed by chemical etching, and the 1100-nm thick KTN film was etched locally by laser ablation. This technique is one of the available processes to remove material from a solid surface [32]. It has been preferred to standard wet-etching process since this is a maskless technology that allows getting fast prototyping results. In this paper, a KrF excimer laser coupled to a workstation with micrometric displacements ($X - Y$ tables) has been used. It is worth noting that the same wavelength is used to grow the ferroelectric layer on the substrate and to locally remove it. KTN material interacts efficiently with KrF laser beam due to its optical band gap ($E_g = 4.1$ eV) lower than the photon energy, and its high absorption coefficient ($\alpha > 200\,000$ cm^{-1} at 248 nm). Moreover, sapphire substrate is transparent at this working wavelength. The pattern of the ablated area is controlled through micrometric displacements of the sample under the laser beam. Considering the lateral inhomogeneity of the laser impact, a window stacking and a partial overlapping of the square laser impacts have been carried out to get the cleanest ablated area. The laser fluence was set to 1.5 J/cm², and the number of laser shots/area has been optimized to obtain a clean and smooth ablated zone (40 shots/area). It is worth mentioning that laser microetching can also be applied to other materials (such as BST and STO) with suitable optical properties (i.e., high absorption coefficient at the working laser wavelength), and by adjusting the ablation parameters.

Once KTN has been removed over the predefined zones, the same fabrication steps, as described in Section III-B, were implemented (titanium and silver metallization, photolithography, and wet-etching). Note that a special attention must be taken to align the stub on the nonetched KTN area (100 μm × 1775 μm). The device dimensions are the same as for configuration A. Fig. 3 shows a scanning electron microscopy (SEM) picture of the fabricated device around the ablated zone. The central conductor widths and gaps of the stub and transmission lines are ($w_r = 15$ μm, $g_r = 15$ μm) and ($w = 40$ μm, $g = 45$ μm), respectively.

Additional experimental tests have been implemented using 50 Ω coplanar transmission lines (8-mm length, 40-μm wide with gap of 45 μm) to check that the dielectric characteristics
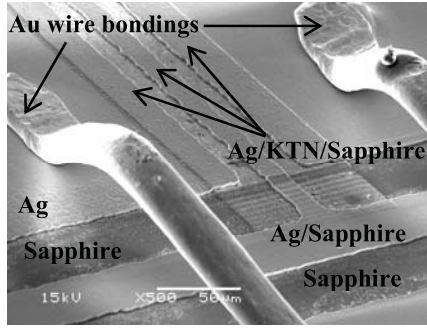
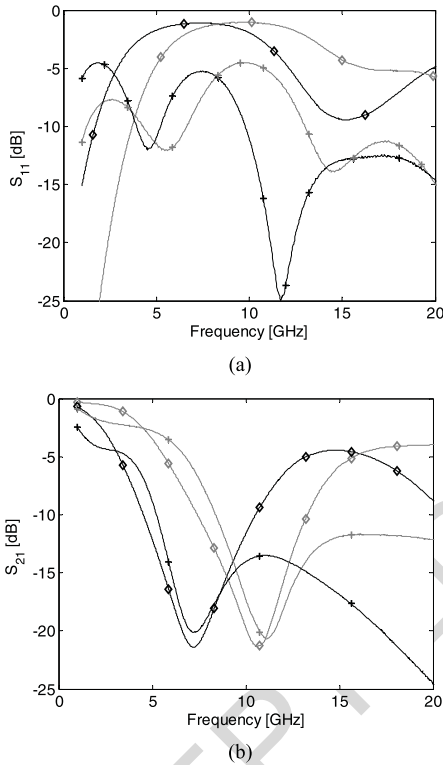Fig. 3. Zoomed-in view close to the tunable stub resonator after microetching of KTN (SEM picture).

(a)

(b)

Fig. 4. Measured reflection and transmission coefficients before [configuration A (+)] and after [configuration B ($\Diamond$)] the KTN laser microetching. Black lines: $E_{bias} = 0$ kV/cm. Grey lines: $E_{bias} = 80$ kV/cm. (a) Reflection coefficient S_{11}. (b) Transmission coefficient S_{21}.

of the initial KTN layer are not affected by silver and titanium chemical etching, and by titanium and silver deposition. The measurement results (not given here) confirm that the KTN layer properties remain the same; this also confirms that we can use the same substrate and KTN layer for a fair comparison between configurations A and B.

IV. MEASUREMENTS

The scattering parameters have been measured at room temperature between 1 and 20 GHz using a vector network analyzer, two bias tees, and a probe station. The maximum dc bias voltage equals 120 V, which corresponds to a maximum static electric field of $E_{bias} = 80$ kV/cm in both slots surrounding the stub resonator.

RESONANCE FREQUENCY F_r, REFLECTION COEFFICIENT S_{11}, GL, AND TUNABILITY T FOR CONFIGURATIONS A AND B (EXPERIMENTAL RESULTS)

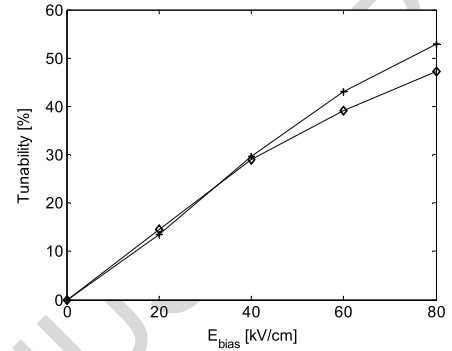| Config.	$E_{bias} = 0$ kV/cm			$E_{bias} = 80$ kV/cm			T (%)
	F_r(GHz)	S_{11} @ F_r (dB)	GL @ F_r	F_r(GHz)	S_{11} @ F_r (dB)	GL @ F_r	
A (ref.)	7.2	-5.3	0.7	11.1	-5.3	0.7	54
B	7.2	-1.1	0.2	10.6	-1.1	0.2	47

Fig. 5. Tunability versus biasing, before [configuration A (+)] and after [configuration B ($\Diamond$)] the KTN laser microetching.

Fig. 4 shows the measured reflection and transmission coefficients of the stub resonator before (configuration A) and after (configuration B) KTN microetching. This figure demonstrates that the resonance frequency can be tuned continuously between 7.2 GHz ($E_{bias} = 0$ kV/cm) and 11.1 GHz ($E_{bias} = 80$ kV/cm) for configuration A, and between 7.2 and 10.6 GHz for configuration B. The corresponding tunability equals $T = 54\%$ and 47%, respectively. The detailed results are summarized in Table III. In configuration A, a strong attenuation of the S_{21} parameter beyond resonance is observed [Fig. 4(b), black line and symbol +]; this comes from the intrinsic loss of the KTN layer [25]. As expected, this attenuation is drastically reduced once KTN is removed locally [Fig. 4(b), black line and symbol $\Diamond$].

Fig. 5 shows the variation of tunability T of configurations A and B as a function of biasing field. Both curves show a linear variation, indicating the nonsaturated state of the ferroelectric material under the maximum biasing field value. The slight reduction of T observed after laser microetching for $E_{bias} > 40$ kV/cm might be due to the slight decrease of the effective permittivity once KTN has been ablated. Indeed, in this case, the effective permittivity is reduced, and consequently its relative variation under biasing becomes smaller, especially for large bias field. This also explains why tunability measured in configuration B is lower than that obtained by numerical simulation (47% against 55%, respectively).

Finally, we compare in Fig. 6 the frequency variations of the GL for the configurations A and B before and after KTN microetching. This figure clearly demonstrates that the total loss is divided by a factor close to 3 when confining KTN only under the stub resonator, with and without biasing.
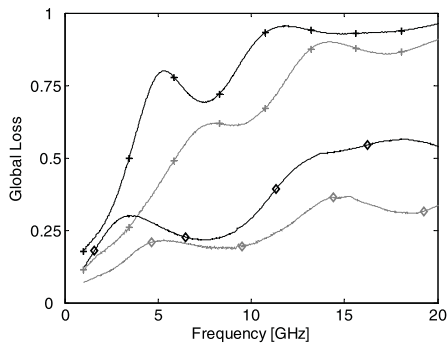
Fig. 6. GL of the stub resonator versus frequency before [configuration A (+)] and after [configuration B ($\Diamond$)] the KTN laser microetching. Black lines: $E_{\text{bias}} = 0$ kV/cm. Grey lines: $E_{\text{bias}} = 80$ kV/cm.

V. CONCLUSION

An original solution aiming at reducing the insertion loss of tunable KTN devices has been proposed. It consists in confining the KTN material only in regions of interest. A specific fabrication process based on laser microetching has been implemented for this purpose. The numerical results have been confirmed experimentally using a simple benchmarking structure, namely, a CPW stub resonator printed on KTN/sapphire. It is demonstrated that local ablation of KTN layer enables to divide the GL by a factor 3.3 at resonance while keeping up a very high-frequency tunability (47%) under a moderate applied electric field.

This solution paves the way for the design and the fabrication of planar ferroelectric tunable devices with lower loss in X-band and better performance at higher frequencies.

REFERENCES

[1] D. Cruickshank, *Microwave Materials for Wireless Applications*, 1st ed. Boston, MA, USA: Artech House, 2011, pp. 175–190.

[2] S. S. Gevorgian, *Ferroelectrics in Microwave Devices, Circuits and Systems*, 1st ed. London, U.K.: Springer-Verlag, 2009, pp. 1–19.

[3] J.-H. Lim, G.-T. Back, Y.-I. Ko, C.-W. Songa, and T.-Y. Yun, "A reconfigurable PIFA using a switchable pin-diode and a fine-tuning varactor for USPCS/WCDMA/m-WiMAX/WLAN," *IEEE Trans. Antennas Propag.*, vol. 58, no. 7, pp. 2404–2411, Jul. 2010.

[4] S. Tanaka, N. Taguchi, T. Kimura, and Y. Atsumi, "Frequency-tunable PIN diode switch for software defined radio," in *Proc. Eur. Wireless Technol. Conf.*, Paris, France, Oct. 2005, pp. 313–316.

[5] A. R. Brown and G. M. Rebeiz, "A varactor-tuned RF filter," *IEEE Trans. Microw. Theory Techn.*, vol. 48, no. 7, pp. 1157–1160, Jul. 2000.

[6] M. A. El-Tanani and G. M. Rebeiz, "A two-pole two-zero tunable filter with improved linearity," *IEEE Trans. Microw. Theory Techn.*, vol. 57, no. 4, pp. 830–839, Apr. 2009.

[7] E. R. Brown, "RF-MEMS switches for reconfigurable integrated circuits," *IEEE Trans. Microw. Theory Techn.*, vol. 46, no. 11, pp. 1868–1880, Nov. 1998.

[8] N. Biyikli, Y. Damgaci, and B. A. Cetiner, "Low-voltage small-size double-arm MEMS actuator," *Electron. Lett.*, vol. 45, no. 7, pp. 354–356, Mar. 2009.

[9] S. Bulja, D. Mirshekar-Syahkal, R. James, S. E. Day, and F. A. Fernandez, "Measurement of dielectric properties of nematic liquid crystals at millimeter wavelength," *IEEE Trans. Microw. Theory Techn.*, vol. 58, no. 12, pp. 3493–3501, Dec. 2010.

[10] N. Tentillier, F. Krasinski, R. Sauleau, B. Splingart, H. Lhermite, and P. Coquet, "A liquid-crystal, tunable, ultra-thin Fabry–Perot resonator in Ka band," *IEEE Antennas Wireless Propag. Lett.*, vol. 8, pp. 701–704, Jun. 2009.

[11] S. S. Gevorgian, *Ferroelectrics in Microwave Devices Circuits and Systems*, 1st ed. London, U.K.: Springer-Verlag, 2009, pp. 175–223.

[12] A. K. Tagantsev, V. O. Sherman, K. F. Astafiev, J. Venkatesh, and N. Setter, "Ferroelectric materials for microwave tunable applications," *J. Electroceram.*, vol. 11, nos. 1–2, pp. 5–66, Nov. 2003.

[13] L. C. Sengupta and S. Sengupta, "Breakthrough advances in low loss, tunable dielectric materials," *Mater. Res. Innov.*, vol. 2, no. 5, pp. 278–282, Apr. 1999.

[14] M. Ouaddari, S. Delprat, F. Vidal, M. Chaker, and K. Wu, "Microwave characterization of ferroelectric thin-film materials," *IEEE Trans. Microw. Theory Techn.*, vol. 53, no. 4, pp. 1390–1397, Apr. 2005.

[15] B. Ouagague *et al.*, "BST tunability study at DC and microwave frequencies by using IDC and MIM capacitors," in *Proc. Asia-Pacific Microw. Conf.*, Yokohama, Japan, Dec. 2010, pp. 1837–1840.

[16] F. A. Houndonougbo *et al.*, "A 380–420 MHz two-pole tunable filter using new ferroelectric composite capacitors," in *Proc. Eur. Microw. Conf.*, Paris, France, Sep. 2010, pp. 1134–1137.

[17] M. Gil *et al.*, "Tunable sub-wavelength resonators based on barium-strontium-titanate thick-film technology," *IET Microw. Antennas Propag.*, vol. 5, no. 3, pp. 316–323, Feb. 2010.

[18] Y. Zheng, M. Sazegar, H. Maune, X. Zhou, J. R. Binder, and R. Jakoby, "Compact substrate integrated waveguide tunable filter based on ferroelectric ceramics," *IEEE Microw. Wireless Compon. Lett.*, vol. 21, no. 9, pp. 477–479, Sep. 2011.

[19] J. Papapolymerou, C. Lugo, Z. Zhao, X. Wang, and A. Hunt, "A miniature low-loss slow-wave tunable ferroelectric bandpass filter from 11–14 GHz," in *IEEE MTT-S Int. Microw. Symp. Dig.*, San Francisco, CA, USA, Jun. 2006, pp. 556–559.

[20] M. W. Cole, P. C. Joshi, M. H. Ervin, M. C. Wood, and R. L. Pfeffer, "The influence of Mg doping on the materials properties of $Ba_{1-x}Sr_xTiO_3$ thin films for tunable device applications," *Thin Solid Films*, vol. 374, no. 1, pp. 34–41, Oct. 2000.

[21] M. Al Ahmad, N. Rolland, and P.-A. Rolland, "Tunable BST capacitor loss compensation using active circuit," *IEEE Microw. Wireless Compon. Lett.*, vol. 16, no. 10, pp. 549–551, Oct. 2006.

[22] D. Rytz, A. Châtelain, and U. T. Höchli, "Elastic properties in quantum ferroelectric $KTa_{1-x}Nb_xO_3$," *Phys. Rev. B*, vol. 27, no. 11, pp. 6830–6840, Jun. 1983.

[23] A. Perrin *et al.*, "Epitaxially grown ferroelectric thin films for agile devices," *Phase Transitions*, vol. 81, nos. 7–8, pp. 643–665, Jul./Aug. 2008.

[24] S. S. Gevorgian and E. L. Kollberg, "Do we really need ferroelectrics in paraelectric phase only in electrically controlled microwave devices?" *IEEE Trans. Microw. Theory Techn.*, vol. 49, no. 11, pp. 2117–2124, Nov. 2001.

[25] Q. Simon *et al.*, "Highly tunable microwave stub resonator on ferroelectric $KTa_{0.5}Nb_{0.5}O_3$ thin film," *Appl. Phys. Lett.*, vol. 99, no. 9, p. 092904, Aug. 2011.

[26] V. Laur *et al.*, "Tunable DBR resonators using KTN ferroelectric thin-films," in *Proc. IEEE/MTT-S Int. Microw. Symp.*, Honolulu, HI, USA, Jun. 2007, pp. 2059–2062.

[27] J. Venkatesh, V. Sherman, and N. Setter, "Synthesis and dielectric characterization of potassium niobate tantalate ceramics," *J. Amer. Ceram. Soc.*, vol. 88, no. 12, pp. 3397–3404, Dec. 2005.

[28] Q. Simon *et al.*, "Reduction of microwave dielectric losses in $KTa_{1-x}Nb_xO_3$ thin films by MgO-doping," *Thin Solid Films*, vol. 517, no. 20, pp. 5940–5942, Aug. 2009.

[29] J.-M. Le Floch, F. Houndonougbo, V. Madrangeas, D. Cros, M. Guilloux-Viry, and W. Peng, "Thin film materials characterization using TE modes cavity," *J. Electromagn. Waves Appl.*, vol. 23, no. 4, pp. 549–559, Feb. 2009.

[30] F. A. Miranda, G. Subramanyam, F. W. Van Keuls, R. R. Romanofsky, J. D. Warner, and C. H. Mueller, "Design and development of ferroelectric tunable microwave components for Ku and K-band satellite communication systems," *IEEE Trans. Microw. Theory Techn.*, vol. 48, no. 7, pp. 1181–1189, Jul. 2000.

[31] A.-G. Moussavou *et al.*, "$KTa_{0.5}Nb_{0.5}O_3$ ferroelectric thin films grown by pulsed laser deposition: Structural characteristics and applications to microwave devices," *Phys. Status Solidi C*, vol. 5, no. 10, pp. 3298–3303, Aug. 2008.

[32] G. Legeay, X. Castel, R. Benzerga, and J. Pinel, "Excimer laser beam/ITO interaction: From laser processing to surface reaction," *Phys. Status Solidi C*, vol. 5, no. 10, pp. 3248–3254, Aug. 2008.